Topological Quantum Optics Using Atomlike Emitter Arrays Coupled to Photonic Crystals

J. Perczel,[1,2,*] J. Borregaard,[2,3] D. E. Chang,[4,5] S. F. Yelin,[2,6] and M. D. Lukin[2]
[1]Physics Department, Massachusetts Institute of Technology, Cambridge, Massachusetts 02139, USA
[2]Physics Department, Harvard University, Cambridge, Massachusetts 02138, USA
[3]QMATH, Department of Mathematical Sciences, University of Copenhagen, Copenhagen 2100, Denmark
[4]ICFO—Institut de Ciencies Fotoniques, The Barcelona Institute of Science and Technology, 08860 Castelldefels, Barcelona, Spain
[5]ICREA—Institució Catalana de Recerca i Estudis Avançats, 08015 Barcelona, Spain
[6]Department of Physics, University of Connecticut, Storrs, Connecticut 06269, USA

(Received 15 April 2019; accepted 11 December 2019; published 25 February 2020)

We propose an experimentally feasible nanophotonic platform for exploring many-body physics in topological quantum optics. Our system is composed of a two-dimensional lattice of nonlinear quantum emitters with optical transitions embedded in a photonic crystal slab. The emitters interact through the guided modes of the photonic crystal, and a uniform magnetic field gives rise to large topological band gaps, robust edge states, and a nearly flat band with a nonzero Chern number. The presence of a topologically nontrivial nearly flat band paves the way for the realization of fractional quantum Hall states and fractional topological insulators in a topological quantum optical setting.

DOI: 10.1103/PhysRevLett.124.083603

Since the discovery of topological phenomena in photonic systems [1,2], analogs of the quantum Hall effect have been explored in a variety of photonic systems, including gyromagnetic photonic crystals [3–6], helical waveguides [7], phase- and time-modulated optical resonators [8–10], polaritons in optical cavities [11], and topological lasers [12–14]. While at microwave frequencies gyromagnetic effects can break time-reversal symmetry [3–6], the same effects become extremely weak at optical frequencies making optical topological systems generally robust only with respect to certain types of disorder [15]. Linear photonic systems also generally lack the interactions between constituent particles required to obtain exotic states of matter such as the fractional quantum Hall effect [16].

Recently, nonlinear quantum emitter arrays in free space were shown to support robust topological states protected by broken time-reversal symmetry at optical frequencies [17–19]. Such an approach requires deeply subwavelength interatomic spacing, which is challenging to implement experimentally [20]. Furthermore, realizing strongly correlated topological many-body physics requires topological bands with negligible dispersion relative to the energy scale of the interactions [21–27]. This is difficult to attain in atomic lattices in free space due to the lack of tunability of the dispersion of the topological bands [18]. Combining nonlinear quantum emitters with nanophotonic systems has recently emerged as a viable route for making system parameters tunable in a wide range [28–33], potentially opening up strongly correlated states of light and matter for experimental realization [34–39]. Pioneering work has demonstrated the coupling of a *single* quantum emitter to a topological photonic interface [40,41], but the development of a truly robust, large-scale many-body platform for topological quantum optics remains an outstanding challenge. Realization of robust topological systems in the optical domain is especially interesting in light of potential applications to quantum networking [42].

In this Letter, we propose an interface between a two-dimensional photonic crystal and an atomic emitter array, which addresses all of the above issues to realize a robust topological system with all necessary ingredients for the realization of strongly correlated topological many-body states at optical frequencies. Specifically, we consider a two-dimensional atomic emitter array integrated with a two-dimensional photonic crystal slab. We show that in the presence of an out-of-plane magnetic field, the hybridization of the atomic levels and the photonic modes of the slab lead to energy bands with nontrivial Chern numbers. In contrast to free-space realizations, we find very large topological band gaps and the existence of an almost completely flat topological band. This makes the system a strong candidate for the realization of fractional phases, such as fractional Chern insulators [21–26]. We also demonstrate the formation of topological edge states that are robust to imperfections in the lattice and inhomogeneous broadening of the emitters. Notably, the required lattice spacing of the emitters is comparable to the optical wavelength, which is an order of magnitude larger than for free-space systems [17–19]. The hybrid approach considered here thus opens up an experimentally accessible

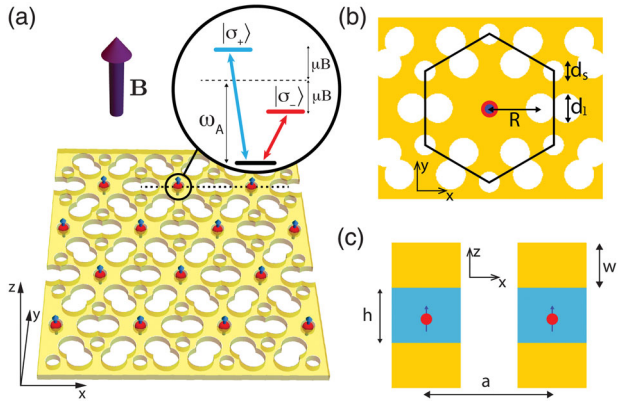

FIG. 1. (a) Schematic depiction of the photonic crystal slab with air holes and the embedded triangular emitter array. Emitter spacing is $a = 240$ nm, transition wavelength is $\lambda = 738$ nm. Out-of-plane B field splits the $|\sigma_+\rangle$ and $|\sigma_-\rangle$ atomic transitions. (b) Unit cell of the photonic crystal (black lines). The emitter is embedded at the center. The diameters of small and large holes are $d_s = 40$ nm and $d_l = 56$ nm, respectively. The large holes are centered $R = 96$ nm away from the emitter. (c) Cross section of the photonic structure along the dotted line indicated in (a). The SiVs are embedded in a diamond ($n_d = 2.4$) layer of thickness $h = 120$ nm, which is surrounded on both sides by GaP ($n_{\mathrm{GaP}} = 3.25$) layers of thickness $w = 75$ nm.

platform for exploring topological quantum optics and many-body physics.

The physical system is depicted in Fig. 1(a). A triangular lattice of quantum emitters (spacing $a = \lambda/3$) is embedded in a two-dimensional photonic crystal (PC) slab of air holes. Each atomic emitter has optical transitions with wavelength λ between the ground state $|g\rangle$ and the two excited states $|\sigma_+\rangle$ and $|\sigma_-\rangle$. The emitters are surrounded by a cavitylike hole structure and interact via the guided modes of the slab. A uniform out-of-plane magnetic field Zeeman splits the excited states of each emitter. The resulting polaritonic bands feature nontrivial Chern numbers and one band is almost completely flat [Fig. 2(b)]. A large energy gap is formed between the bands, which is 2 orders of magnitude larger than the gap in free space for comparable emitter spacings [17,18]. Inside the gap, topological edge states appear, which are protected by the large gap from scattering into extended bulk states or guided modes of the slab.

For concreteness, we focus on the hybrid PC structure illustrated in Fig. 1. The unit cell of the PC slab made of gallium phosphate (GaP) with air holes is shown in Fig. 1(b). Each atomic emitter is placed at the geometric center of the unit cell, forming a periodic triangular lattice. The emitters are placed in the middle of the slab ($z = 0$ mirror plane) to ensure that they only couple to TE-like guided modes [43]. This can be achieved for different kinds of quantum emitters by introducing slight modifications to the PC structure. One option is to embed quantum dots directly into the dielectric slab [41,44–48]. Another option is to create an additional hole at the center of the cell and trap there a neutral atom using far-off-resonance optical trapping, vacuum forces, and side illumination [35]. Alternatively, atomlike color defects in diamond such as silicon vacancy (SiV) centers can be integrated with the photonic structure [49–51] using a thin diamond layer sandwiched between two layers of GaP, as shown in Fig. 1(c). For the calculations below, we focus on an implementation with SiV centers.

The TE-like guided bands of the slab near the emitter frequency are shown in Fig. 2(a) [52]. The colors of the bands indicate the normalized field strength $|\mathbf{E}_{\mathbf{k}}(\mathbf{r}_A)|^2 a^3$ at the location of the emitter inside the unit cell where $\mathbf{E}_{\mathbf{k}}(\mathbf{r})$ denotes the classical field solutions of Maxwell's equations for Bloch quasimomentum $\mathbf{k}$ [43,52–54]. This photonic structure was designed to ensure that there are no other guided modes within a few terahertz energy range just below the tip of the Dirac cone. Such a spectrum is a general feature of PC slabs with the cavitylike hole structure shown in Fig. 1(b) and can be achieved for a wide range of parameters [55]. The thickness of the layers and the size and spacing of the holes of the diamond-GaP structure are chosen such that the tip of the Dirac cone ω_{Dirac} is tuned within a few hundred gigahertz of $\omega_A = 2\pi c/\lambda$, the SiV transition frequency ($\lambda = 738$ nm).

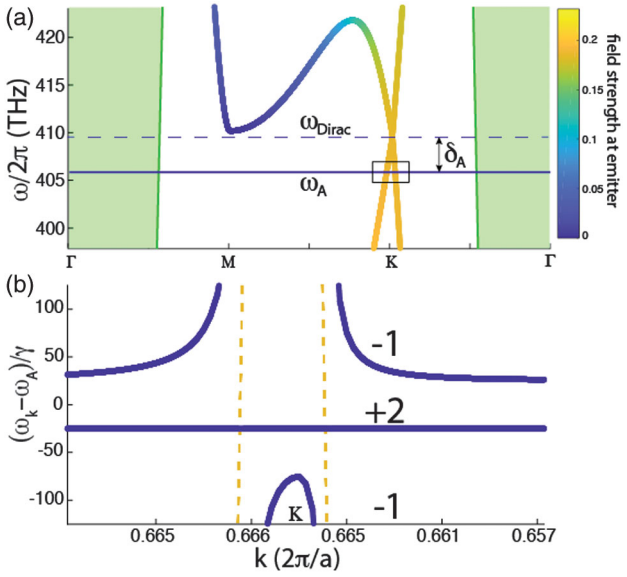

FIG. 2. (a) TE-like photonic band structure of the slab in the vicinity of the SiV transition frequency ω_A. The light cone region is shaded green. The tip of the Dirac cone ω_{Dirac} is detuned by $\delta_A = \omega_{\mathrm{Dirac}} - \omega_A = 3.74$ THz from ω_A. Band colors reflect the normalized field strength $|\mathbf{E}_{\mathbf{k}}(\mathbf{r}_A)|^2 a^3$ at the emitter location. (b) Hybrid atomic-photonic bands in the presence of an out-of-plane B field ($\mu B = 25\gamma$) in the immediate vicinity of the $\mathbf{K}$ point [see black box in (a)] for a detuning of $\delta_A = 0.321$ THz. Yellow dashed lines indicate the bare photonic bands for reference. Chern numbers of the bands are indicated by black numbers.

Thus, the emitters interact primarily through the guided modes of the Dirac cone.

In what follows, we assume that there is a single excitation in the system. The dynamics in the presence of a magnetic field is captured by the non-Hermitian Hamiltonian [17,18,56–59],

$$H = \hbar \sum_{i=1}^{N} \sum_{\alpha=\sigma_+,\sigma_-} \left(\omega_A + \mathrm{sgn}(\alpha_i)\mu B - i\frac{\Gamma}{2}\right) |\alpha_i\rangle\langle\alpha_i| + \frac{3\pi\gamma\hbar c}{\omega_A n_d} \sum_{i\neq j} \sum_{\alpha,\beta=\sigma_+,\sigma_-} G_{\alpha\beta}(\mathbf{r}_i - \mathbf{r}_j)|\alpha_i\rangle\langle\beta_j|, \quad (1)$$

where N is the number of emitters, $\mathrm{sgn}(\sigma_\pm) = \pm$, μB is the Zeeman shift of the emitters with magnetic moment μ due to the magnetic field $\mathbf{B} = B\hat{z}$, γ is the emission rate of SiVs in bulk diamond, c is the speed of light, and n_d is the refractive index of diamond.

Since we only consider a single excitation in the system, the effect of any quantum jump operators would be to prepare all spins in the ground state from which no further evolution is possible. The rate of such quantum jumps is equal to the rate of population loss of the wave function evolving under H [60]. Thus, this Hamiltonian effectively captures the effect of any quantum jumps. For further details on the physical motivation of the Hamiltonian, see Refs. [61–66].

The dipolar spin-spin interaction of the emitters is described by the dyadic Green's function $G_{\alpha\beta}(\mathbf{r})$ where $\mathbf{r}_i$ denotes the position of the ith atom. The irreversible decay rate of individual emitters inside the slab is $\Gamma = \Gamma_{\mathrm{PC}} + \Gamma_0$, where Γ_{PC} (Γ_0) accounts for scattering into guided slab (free-space) modes. In general, $\Gamma_0 \ll \gamma$ due to total internal reflection [47] and we therefore neglect coupling to free-space modes for now (see Ref. [52] for further discussion).

The single excitation eigenmodes of Eq. (1) are Bloch modes of the form

$$|\psi_{\mathbf{k}}\rangle = \sum_n e^{i\mathbf{k}\cdot\mathbf{R}_n}[c_{+,\mathbf{k}}|\sigma_{+,n}\rangle + c_{-,\mathbf{k}}|\sigma_{-,n}\rangle], \quad (2)$$

where the summation runs over all lattice vectors $\{\mathbf{R}_n\}$ and $\mathbf{k}$ is the Bloch quasimomentum. For each $\mathbf{k}$, there are two eigenvalues $\omega_{\mathbf{k}}$ that can be numerically calculated from the photonic band structure shown in Fig. 2(a) [52]. Figure 2(b) shows the hybridized bands in the vicinity of the $\mathbf{K}$ symmetry point in the presence of an out-of-plane magnetic field. One atomic band does not interact with the guided slab modes due to polarization mismatch, forming a flatband in the middle. The other atomic band hybridizes with the guided modes, forming avoided crossings that split the band into two disjoint parts. Two equal band gaps form above and below the middle band and the three bands have Chern numbers -1, $+2$, and -1, respectively.

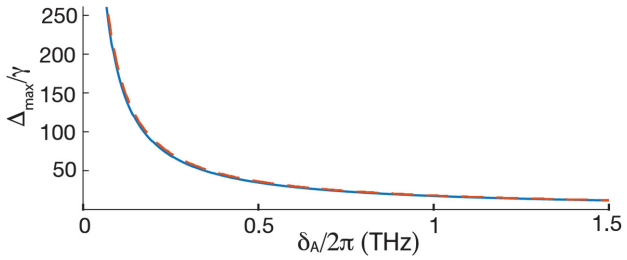

FIG. 3. Maximum gap size Δ_{max} as a function of the detuning δ_A (blue line). The dashed red line is a $\sim 1/\delta_A$ fit.

The topological protection of the system increases with gap size Δ. Because of the Zeeman splitting of the atomic levels, the gap size increases linearly with the applied magnetic field [17], until the middle band completely flattens and the maximum gap size Δ_{max} is achieved [52]. The maximum gap size is plotted in Fig. 3 as a function of the detuning $\delta_A = \omega_{\mathrm{Dirac}} - \omega_A$ between the tip of the Dirac cone and the atomic transition frequency. As the tip of the Dirac cone is tuned closer to the emitter frequency, the energy gap increases as $\sim 1/\delta_A$. This stands in contrast with the free-space results, where increasing the gap size required reducing the interatomic distance [17]. Ultimately, the gap size is limited by the fact that our quantum optical model relies on the Markov approximation [67] and is only valid as long as the emitter-field correlation time τ_c is much shorter than the typical timescale on which the emitter system evolves (see Ref. [52] for details).

We next explore the topological edge states of the system considering a small gap size (i.e., large δ_A) to ensure sufficient density of states near the tip of the Dirac cone even for limited lattice sizes. For edge state calculations corresponding to the parameters of Fig. 2 and analysis of the system evolution when the density of states is low, refer to Ref. [52].

First, we consider a stripe of emitters, embedded in an extended PC, that is infinite along the y axis, but finite along the x axis as shown in Fig. 4(a). Figure 4(b) shows the unidirectional edge states inside the gap near the $\mathbf{K}$ point. These states are confined to the system boundaries and carry energy only in one direction due to the broken time-reversal symmetry and the topological protection of the system [1–3,17,18,68,69]. Edge states that fall within the quasimomentum region where the guided modes of the Dirac cone are resonant with the emitters [yellow region in Fig. 4(b)] have a decay rate of $\Gamma_{\mathrm{PC}} = \mathrm{Im}(\omega_{\mathbf{k}})$ from coupling to guided slab modes. This decay significantly broadens the energy levels of these states, making their frequency and slope ill defined. Near the center of this region, the width of the edge modes far exceeds the size of the gap ($\Gamma_{\mathrm{PC}} \gg \gamma$), effectively connecting the edge states to the upper band, making the spectrum gapless. Modes outside the yellow region cannot couple to slab modes due to the momentum mismatch, making these modes long-lived ($\Gamma_{\mathrm{PC}} \approx 0$).

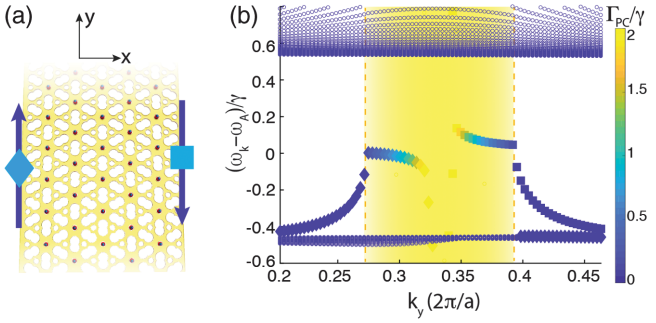

FIG. 4. (a) Infinite stripe of emitters embedded in an extended photonic crystal slab. (b) Edge states inside the band gap near the **K** point. Unidirectional edge states on the left (right) boundary are indicated by diamonds (squares). Bulk modes are marked by dots, which form a nearly flat band inside the gap. Yellow shading and yellow dashed lines mark the region where bands can decay into resonant slab modes. Color coding shows the decay rate Γ_{PC}. Relevant parameters are $\delta_A = 18.73$ THz, $v_s = 0.25c$, $|E_0|^2 = 0.1855/a^3$, $\Delta = \gamma$, and $\mu B = 0.5\gamma$. Results were obtained for a stripe with 81 atoms in the transverse direction. States with 5 times more amplitude on the five leftmost emitter columns than on the five rightmost columns are classified as edge states.

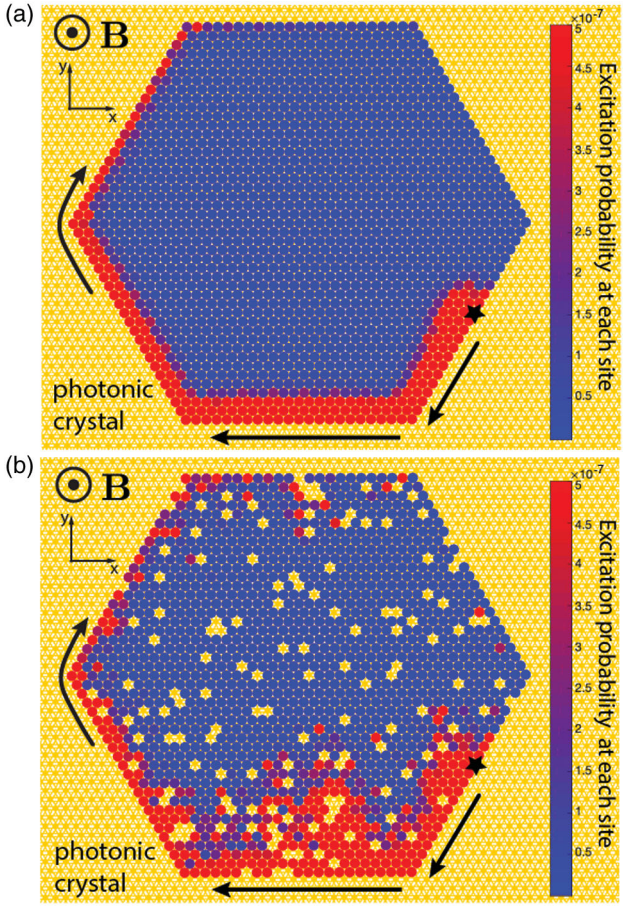

FIG. 5. (a) Time-evolved state ($t = 161.5\gamma^{-1}$) of a hexagonal-shaped triangular lattice of emitters ($N = 1519$) embedded in an extended photonic crystal slab. An emitter at the edge is addressed by a laser (black star). The edge state propagates on the boundaries without reflection or significant decay into slab modes. The color code shows the excitation probability at each emitter. (b) Time-evolved state ($t = 297.5\gamma^{-1}$) of the system ($N = 1380$) in the presence of imperfect lattice filling (90%) and inhomogeneous broadening, where the emitter frequencies are sampled from $P(\omega) = 1/\sqrt{2\pi\sigma^2}\exp[-(\omega-\omega_A)^2/(2\sigma^2)]$, where $\sigma = 0.1\Delta$. Other relevant parameters are $\delta_A/2\pi = 18.73$ THz, $v_s = 0.25c$, $|E_0|^2 = 0.1855/a^3$, $\Delta = \gamma$, $\mu B = 0.5\gamma$, $\Omega = 0.0059\gamma$, and $\omega_L = \omega_A - 0.37\gamma$. The laser drive is switched on adiabatically with the profile $\Omega(t) = \Omega\exp(-[t-t_0]^2/[2\Sigma^2])$, where $t_0 = 127.5\gamma^{-1}$ and $\Sigma = 23.3\gamma^{-1}$.

Next, we study the time evolution of edge states in real space. Figure 5(a) shows a defect-free triangular lattice of emitters embedded in an extended PC. One emitter on the edge is driven by a weak laser with frequency ω_L resonant with the edge states in the lower half of the gap. The laser drives the σ_+ and σ_- transitions with equal strength Ω, such that $\Omega \ll \Delta$. We calculate the time evolution of the wave function of the initial state by numerically exponentiating Eq. (1) [18] and observing that the only relevant timescale for the system evolution is γ^{-1}. The state of the system at one particular time is shown in Fig. 5(a). The edge states carry energy only in the clockwise direction due to broken time-reversal symmetry by the out-of-plane B field, and coupling to bulk modes is strongly suppressed. The excitation routes around the lattice corners without reflection or significant loss into the guided modes of the slab.

The hallmark of topological edge states is their robustness to imperfections. Figure 5(b) shows a lattice, where a random 10% of the emitters is missing and we account for inhomogeneous broadening of emitters (e.g., due to fabrication imperfections) by sampling the emitter frequencies from a Gaussian distribution, whose width is 10% of the gap. Figure 5(b) shows a snapshot of the time-evolved system. Despite the lattice defects and inhomogeneous broadening, the edge state propagates along the system edges, routing around all defects. These results demonstrate the topological robustness of the edge states.

The flat middle band in Fig. 2(b) is a key feature of our topological system. The flatness of the band and the nontrivial Chern number are the two key ingredients for fractionalized topological phases in lattice models [21–26,70–72]. Usually, such flatbands require careful tuning of the long-range hopping parameters. Here, the band remains flat away from the K point as the guided photonic bands are far detuned and coupling to them is weak [Fig. 2(a)]. Near the **K** point, flatness arises from the combined effects of the uniform magnetic field and the fact that the middle band does not couple to the PC bands due to polarization mismatch. The inherent nonlinearity of the constituent emitters gives rise to a hard-core constraint for the bosonic excitations of the system, which provides a pointlike interaction for the excitations. Such short-range

interactions are ideal for the realization of interacting many-body topological phases [73]. Within such a system, we expect nontrivial competition between states with strongly correlated topological phases and those that behave analogously to electronic charge density waves. This competition arises from the fact that the atoms interact primarily through the Dirac cone and, therefore, the Berry curvature is concentrated in the vicinity of the **K** points. Thus, only states near the **K** points are expected to yield exotic topological many-body phases, whereas the rest of the band will likely contribute to states that resemble an ordered quantum fluid. Controlling the distribution of the Berry curvature in the flatband (e.g., using established techniques from cold atom experiments [74]) can be explored for engineering experimentally observable fractional topological phases.

While practical realization of the proposed systems constitutes a nontrivial challenge, most of the key ingredients have already been demonstrated. For example, a hybrid system based on SiV color defects in diamond can be created by first fabricating a thin diamond slab [49,75], SiVs can be implanted using focused ion beam implantation [76], while GaP can be positioned on both sides of the slab [77] with the air-hole structure created by etching through the GaP and diamond layers. Alternatively, a PC hole structure made entirely of diamond can potentially be used (see Ref. [52] for more details).

We have demonstrated that, under realistic experimental parameters, two-dimensional quantum emitter arrays embedded in photonic crystals constitute a topological quantum optical system with long-lived topologically robust edge states and a flatband with a nontrivial Chern number. We believe that the experimental accessibility of this platform and its suitability for engineering many-body interactions will open up exciting opportunities for exploring novel topological states of light and matter, including quantum optical analogs of fractional Chern insulators.

We would like to thank Mihir Bhaskar, Ruffin Evans, Alejandro González-Tudela, Fabian Grusdt, Bert Halperin, Hannes Pichler, Denis Sukachev, Efraim Shahmoon, Dominik Wild, Bihui Zhu, and Peter Zoller for valuable discussions. This work was supported through the National Science Foundation (NSF), the MIT-Harvard Center for Ultracold Atoms, the Air Force Office of Scientific Research via the MURI, the Vannevar Bush Faculty Fellowship, and DOE. Some of the computations in this Letter were performed on the Odyssey cluster supported by the FAS Division of Science, Research Computing Group at Harvard University. J. P. acknowledges support from the Dr. Elemér and Éva Kiss Scholarship Fund. J. B. acknowledges support from the European Research Council (ERC Grant Agreement No. 337603) and VILLUM FONDEN via the QMATH Centre of Excellence (Grant No. 10059). D. E. C. acknowledges support from the ERC Starting Grant FOQAL, MINECO Plan Nacional Grant CANS, MINECO Severo Ochoa Grant No. SEV-2015-0522, CERCA Programme/Generalitat de Catalunya, Fundacio Privada Cellex, and AGAUR Grant No. 2017 SGR 1334.

*jperczel@fas.harvard.edu

[1] F. D. M. Haldane and S. Raghu, Phys. Rev. Lett. **100**, 013904 (2008).
[2] S. Raghu and F. D. M. Haldane, Phys. Rev. A **78**, 033834 (2008).
[3] Z. Wang, Y. D. Chong, J. D. Joannopoulos, and M. Soljačić, Phys. Rev. Lett. **100**, 013905 (2008).
[4] K. Liu, L. Shen, and S. He, Opt. Lett. **37**, 4110 (2012).
[5] Z. Wang, Y. Chong, J. D. Joannopoulos, and M. Soljačić, Nature (London) **461**, 772 (2009).
[6] Z. Yu, G. Veronis, Z. Wang, and S. Fan, Phys. Rev. Lett. **100**, 023902 (2008).
[7] M. C. Rechtsman, J. M. Zeuner, Y. Plotnik, Y. Lumer, D. Podolsky, F. Dreisow, S. Nolte, M. Segev, and A. Szameit, Nature (London) **496**, 196 (2013).
[8] M. Hafezi, E. A. Demler, M. D. Lukin, and J. M. Taylor, Nat. Phys. **7**, 907 (2011).
[9] M. Hafezi, S. Mittal, J. Fan, A. Migdall, and J. M. Taylor, Nat. Photonics **7**, 1001 (2013).
[10] K. Fang, Z. Yu, and S. Fan, Nat. Photonics **6**, 782 (2012).
[11] T. Karzig, C.-E. Bardyn, N. H. Lindner, and G. Refael, Phys. Rev. X **5**, 031001 (2015).
[12] L. Pilozzi and C. Conti, Phys. Rev. B **93**, 195317 (2016).
[13] M. Segev, M. A. Bandres, G. Harari, Y. Plotnik, H. Herzig-Sheinfux, E. Lustig, R. Bekenstein, and M. C. Rechtsman, in *Frontiers in Optics 2016* (Optical Society of America, Washington, DC, 2016), p. LF5I.3.
[14] P. St-Jean, V. Goblot, E. Galopin, A. Lemaıtre, T. Ozawa, L. Le Gratiet, I. Sagnes, J. Bloch, and A. Amo, Nat. Photonics **11**, 651 (2017).
[15] L. Lu, J. D. Joannopoulos, and M. Soljačić, Nat. Photonics **8**, 821 (2014).
[16] R. B. Laughlin, Phys. Rev. Lett. **50**, 1395 (1983).
[17] J. Perczel, J. Borregaard, D. E. Chang, H. Pichler, S. F. Yelin, P. Zoller, and M. D. Lukin, Phys. Rev. Lett. **119**, 023603 (2017).
[18] J. Perczel, J. Borregaard, D. E. Chang, H. Pichler, S. F. Yelin, P. Zoller, and M. D. Lukin, Phys. Rev. A **96**, 063801 (2017).
[19] R. J. Bettles, J. Minář, C. S. Adams, I. Lesanovsky, and B. Olmos, Phys. Rev. A **96**, 041603(R) (2017).
[20] I. Bloch, Nat. Phys. **1**, 23 (2005).
[21] T. Neupert, L. Santos, C. Chamon, and C. Mudry, Phys. Rev. Lett. **106**, 236804 (2011).
[22] E. Tang, J.-W. Mei, and X.-G. Wen, Phys. Rev. Lett. **106**, 236802 (2011).
[23] K. Sun, Z. Gu, H. Katsura, and S. Das Sarma, Phys. Rev. Lett. **106**, 236803 (2011).
[24] N. Y. Yao, C. R. Laumann, A. V. Gorshkov, S. D. Bennett, E. Demler, P. Zoller, and M. D. Lukin, Phys. Rev. Lett. **109**, 266804 (2012).

[25] N. Y. Yao, A. V. Gorshkov, C. R. Laumann, A. M. Läuchli, J. Ye, and M. D. Lukin, Phys. Rev. Lett. **110**, 185302 (2013).

[26] D. Peter, N. Y. Yao, N. Lang, S. D. Huber, M. D. Lukin, and H. P. Büchler, Phys. Rev. A **91**, 053617 (2015).

[27] A. J. Kollár, M. Fitzpatrick, and A. A. Houck, Nature (London) **571**, 45 (2019).

[28] J. D. Thompson, T. G. Tiecke, N. P. de Leon, J. Feist, A. V. Akimov, M. Gullans, A. S. Zibrov, V. Vuletic, and M. D. Lukin, Science **340**, 1202 (2013).

[29] T. G. Tiecke, J. D. Thompson, N. P. de Leon, L. R. Liu, V. Vuletić, and M. D. Lukin, Nature **508**, 241 (2014).

[30] J. D. Hood, A. Goban, A. Asenjo-Garcia, M. Lu, S.-P. Yu, D. E. Chang, and H. J. Kimble, Proc. Natl. Acad. Sci. U.S.A. **113**, 10507 (2016).

[31] A. Goban, C.-L. Hung, J. D. Hood, S.-P. Yu, J. A. Muniz, O. Painter, and H. J. Kimble, Phys. Rev. Lett. **115**, 063601 (2015).

[32] A. Goban, C.-L. Hung, S.-P. Yu, J. D. Hood, J. A. Muniz, J. Lee, M. Martin, A. McClung, K. Choi, D. Chang, O. Painter, and H. J. Kimble, Nat. Commun. **5**, 3808 (2014).

[33] S.-P. Yu, J. D. Hood, J. A. Muniz, M. J. Martin, R. Norte, C.-L. Hung, S. M. Meenehan, J. D. Cohen, O. Painter, and H. J. Kimble, Appl. Phys. Lett. **104**, 111103 (2014).

[34] I. Carusotto and C. Ciuti, Rev. Mod. Phys. **85**, 299 (2013).

[35] A. González-Tudela, C.-L. Hung, D. E. Chang, J. I. Cirac, and H. J. Kimble, Nat. Photonics **9**, 320 (2015).

[36] J. S. Douglas, H. Habibian, C.-L. Hung, A. V. Gorshkov, H. J. Kimble, and D. E. Chang, Nat. Photonics **9**, 326 (2015).

[37] P. Lodahl, S. Mahmoodian, S. Stobbe, A. Rauschenbeutel, P. Schneeweiss, J. Volz, H. Pichler, and P. Zoller, Nature (London) **541**, 473 (2017).

[38] D. G. Angelakis, in *Quantum Science and Technology*, edited by D. G. Angelakis (Springer International Publishing, Cham, 2017), p. 214.

[39] J. I. Cirac and H. J. Kimble, Nat. Photonics **11**, 18 (2017).

[40] S. Barik, H. Miyake, W. DeGottardi, E. Waks, and M. Hafezi, New J. Phys. **18**, 113013 (2016).

[41] S. Barik, A. Karasahin, C. Flower, T. Cai, H. Miyake, W. DeGottardi, M. Hafezi, and E. Waks, Science **359**, 666 (2018).

[42] N. Sangouard, C. Simon, H. de Riedmatten, and N. Gisin, Rev. Mod. Phys. **83**, 33 (2011).

[43] J. D. Joannopoulos, S. G. Johnson, J. N. Winn, and R. D. Meade, in *Photonic Crystals: Molding the Flow of Light*, 2nd ed. (Princeton University Press, Princeton, NJ, 2008), p. 446.

[44] A. Javadi, I. Söllner, M. Arcari, S. L. Hansen, L. Midolo, S. Mahmoodian, G. Kiršanskė, T. Pregnolato, E. H. Lee, J. D. Song, S. Stobbe, and P. Lodahl, Nat. Commun. **6**, 8655 (2015).

[45] S. Sun, H. Kim, G. S. Solomon, and E. Waks, Nat. Nanotechnol. **11**, 539 (2016).

[46] P. Lodahl, S. Mahmoodian, and S. Stobbe, Rev. Mod. Phys. **87**, 347 (2015).

[47] M. Arcari, I. Söllner, A. Javadi, S. Lindskov Hansen, S. Mahmoodian, J. Liu, H. Thyrrestrup, E. H. Lee, J. D. Song, S. Stobbe, and P. Lodahl, Phys. Rev. Lett. **113**, 093603 (2014).

[48] I. Söllner, S. Mahmoodian, S. L. Hansen, L. Midolo, A. Javadi, G. Kiršanskė, T. Pregnolato, H. El-Ella, E. H. Lee, J. D. Song, S. Stobbe, and P. Lodahl, Nat. Nanotechnol. **10**, 775 (2015).

[49] A. Faraon, C. Santori, Z. Huang, V. M. Acosta, and R. G. Beausoleil, Phys. Rev. Lett. **109**, 033604 (2012).

[50] J. Riedrich-Möller, C. Arend, C. Pauly, F. Mücklich, M. Fischer, S. Gsell, M. Schreck, and C. Becher, Nano Lett. **14**, 5281 (2014).

[51] A. Sipahigil, R. E. Evans, D. D. Sukachev, M. J. Burek, J. Borregaard, M. K. Bhaskar, C. T. Nguyen, J. L. Pacheco, H. A. Atikian, C. Meuwly, R. M. Camacho, F. Jelezko, E. Bielejec, H. Park, M. Lončar, and M. D. Lukin, Science **354**, 847 (2016).

[52] See Supplemental Material at http://link.aps.org/supplemental/10.1103/PhysRevLett.124.083603 for more details about the calculations and approximations used in this paper.

[53] R. J. Glauber and M. Lewenstein, Phys. Rev. A **43**, 467 (1991).

[54] J. Perczel, P. Kómár, and M. D. Lukin, Phys. Rev. A **98**, 033803 (2018).

[55] J. Perczel and M. D. Lukin, arXiv:1810.12815.

[56] M. Antezza and Y. Castin, Phys. Rev. Lett. **103**, 123903 (2009).

[57] E. Shahmoon, D. S. Wild, M. D. Lukin, and S. F. Yelin, Phys. Rev. Lett. **118**, 113601 (2017).

[58] T. Bienaimé, N. Piovella, and R. Kaiser, Phys. Rev. Lett. **108**, 123602 (2012).

[59] W. Guerin, M. O. Araújo, and R. Kaiser, Phys. Rev. Lett. **116**, 083601 (2016).

[60] M. T. Manzoni, M. Moreno-Cardoner, A. Asenjo-Garcia, J. V. Porto, A. V. Gorshkov, and D. E. Chang, New J. Phys. **20**, 083048 (2018).

[61] H. T. Dung, L. Knöll, and D.-G. Welsch, Phys. Rev. A **57**, 3931 (1998).

[62] H. T. Dung, L. Knöll, and D.-G. Welsch, Phys. Rev. A **66**, 063810 (2002).

[63] S. Y. Buhmann, L. Knöll, D.-G. Welsch, and H. T. Dung, Phys. Rev. A **70**, 052117 (2004).

[64] S. Y. Buhmann and D.-G. Welsch, Prog. Quantum Electron. **31**, 51 (2007).

[65] S. Scheel and S. Y. Buhmann, Acta Phys. Slovaca **58**, 675 (2008).

[66] S. Y. Buhmann, *Dispersion Forces I*, Springer Tracts in Modern Physics (Springer, Berlin, 2012), Vol. 247.

[67] A. González-Tudela and J. I. Cirac, Phys. Rev. A **97**, 043831 (2018).

[68] R. B. Laughlin, Phys. Rev. B **23**, 5632 (1981).

[69] B. I. Halperin, Phys. Rev. B **25**, 2185 (1982).

[70] Y.-F. Wang, H. Yao, C.-D. Gong, and D. N. Sheng, Phys. Rev. B **86**, 201101(R) (2012).

[71] S. Yang, Z.-C. Gu, K. Sun, and S. Das Sarma, Phys. Rev. B **86**, 241112(R) (2012).

[72] M. Trescher and E. J. Bergholtz, Phys. Rev. B **86**, 241111 (R) (2012).

[73] Z.-X. Gong, M. F. Maghrebi, A. Hu, M. L. Wall, M. Foss-Feig, and A. V. Gorshkov, Phys. Rev. B **93**, 041102(R) (2016).

[74] Y.-C. He, F. Grusdt, A. Kaufman, M. Greiner, and A. Vishwanath, Phys. Rev. B **96**, 201103(R) (2017).

[75] N. H. Wan, S. Mouradian, and D. Englund, Appl. Phys. Lett. **112**, 141102 (2018).
[76] J. L. Pacheco, M. Singh, D. L. Perry, J. R. Wendt, G. Ten Eyck, R. P. Manginell, T. Pluym, D. R. Luhman, M. P. Lilly, M. S. Carroll, and E. Bielejec, Rev. Sci. Instrum. **88**, 123301 (2017).
[77] A. Aparna, V. Brahmajirao, and T. Karthikeyan, Procedia Materials Science **6**, 1650 (2014).